NANO LETTERS

2006
Vol. 6, No. 5
984−994

Exciton–Plasmon Interaction and Hybrid Excitons in Semiconductor–Metal Nanoparticle Assemblies

Alexander O. Govorov,*,† Garnett W. Bryant,‡ Wei Zhang,† Timur Skeini,† Jaebeom Lee,§ Nicholas A. Kotov,§ Joseph M. Slocik,|| and Rajesh R. Naik||

Department of Physics and Astronomy, Ohio University, Athens, Ohio 45701, Quantum Processes and Metrology Group, National Institute of Standards and Technology, Atomic Physics Division, 100 Bureau Drive, Stop 8423, Gaithersburg, Maryland 20899-8423, Department of Chemical Engineering, Biomedical Engineering, and Material Sciences and Engineering, University of Michigan, Ann Arbor, Michigan 48109, and Materials and Manufacturing Directorate, Air Force Research Laboratory, WPAFB, Dayton, Ohio 45433-7702

Received January 29, 2006; Revised Manuscript Received March 26, 2006

ABSTRACT

We describe the physical properties of excitons in hybrid complexes composed of semiconductor and metal nanoparticles. The interaction between individual nanoparticles is revealed as an enhancement or suppression of emission. Enhanced emission comes from electric field amplified by the plasmon resonance, whereas emission suppression is a result of energy transfer from semiconductor to metal nanoparticles. The emission intensity and energy transfer rate depend strongly on the geometrical parameters of the superstructure and the physical and material properties of the nanoparticles. In particular, the emission enhancement effect appears for nanoparticles with relatively small quantum yield, and silver nanoparticles have stronger enhancement compared to gold ones. Using realistic models, we review and analyze available experimental data on energy transfer between nanoparticles. In hybrid superstructures conjugated with polymer linkers, optical emission is sensitive to environmental parameters such as, for example, temperature. This sensitivity comes from expansion or contraction of a linker. With increasing temperature, emission of polymer-conjugated complexes can decrease or increase depending on the organization of a superstructure. The structures described here have potential as sensors and actuators.

1. Introduction. Novel materials can be assembled from nanoscale building blocks such as nanoparticles (NPs), nanowires (NWs), and biolinkers.[1−5] One of the central problems related to these bioassembled structures is the interaction between the nanoscale building blocks. If individual nanoparticles do not exchange carriers, then the interparticle Coulomb interaction becomes the main mechanism of coupling and can strongly change the physical properties of the bioassembly. In particular, these changes can be observed in optical experiments on strongly packed NP and NW superstructures. In the presence of optical excitation, the Coulomb (dipole−dipole) interaction results in inter-NP/NW energy transfer[3−9] and electromagnetic enhancement.[4,10−12] The energy transfer effect is observed as directional flow of excitons between nanocrystals[6,13] or dissipation of exciton energy in the presence of metal NPs.[3,7−9] The electromagnetic enhancement reveals itself as surface-enhanced Raman scattering (SERS)[12] or a strong increase of emission.[4,10,11,14]

Here we study theoretically the interaction between semiconductor and metal nanoparticles (SNPs and MNPs) assembled into superstructures. Elementary excitations in a SNP and MNP, an exciton and a plasmon, have very different properties, and therefore the interaction between them is an interesting problem. In these superstructures, a SNP plays the role of quantum emitter, whereas the MNPs play the role of amplifier or damper. The optical properties of the superstructure become strongly altered compared to single NPs. In most cases, emission of SNP is reduced in the presence of MNPs because of energy dissipation in the metal. However, we find special conditions under which emission of a SNP increases in the presence of MNPs that comes from amplification of the electric field inside a complex. The regime of increased emission can be realized via enhancement of optical absorption or via amplification of the emission process. The first case can be achieved in silver-based structures, whereas the second regime is more typical for the gold−NP assemblies. We also review experimental results obtained by several groups for the gold-based

* Corresponding author. E-mail: Govorov@ohiou.edu.
† Ohio University.
‡ National Institute of Standards and Technology.
§ University of Michigan.
|| WPAFB.

10.1021/nl0602140 CCC: $33.50 © 2006 American Chemical Society
Published on Web 04/15/2006

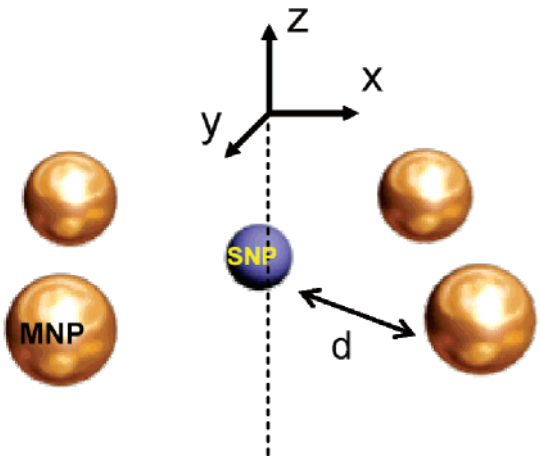

Figure 1. Schematics of a complex composed of metal and semiconductor nanoparticles. *d* denotes a typical distance between SNP and MNPs.

structures.[3,7,9,14] With our numerical formalism, the energy relaxation rate and enhancement factors are calculated beyond the dipole−dipole approximation, which is necessary for densely packed superstructures.

2. Formalism. Here, we present a numerical description for the optical properties of a complex composed of a single SNP and a number, N_γ, of MNPs (Figure 1), where γ denotes a type of metal and can be Au or Ag. The photoluminescence intensity of the semiconductor component depends on the absorption, emission, and energy dissipation rates in the complex. Within the simplest rate model, the number of excitons (n_{exc}) trapped in the SNP is given by the equation: $dn_{exc}/dt = -\gamma_{tot}\cdot n_{exc} + I_{abs}$, where I_{abs} is the intensity of light absorption in the SNP and t is the time. The exciton-recombination rate, γ_{tot}, can be split into three terms: $\gamma_{tot} = \gamma_{rad} + \gamma^0_{non-rad} + \gamma_{non-rad,metal}$, where $\gamma_{rad}(\gamma^0_{non-rad})$ are intra-NP radiative (nonradiative) rates, and $\gamma_{non-rad,metal}$ is the exciton recombination rate of a SNP due to energy transfer to the MNPs. The above model assumes fast relaxation of an excited exciton toward its ground state. Under constant illumination, the steady-state solution is $n_{exc} = I_{abs}/\gamma_{tot}$ and the corresponding quantum yield of the SNP (quantum dot) is given by $Y = \gamma_{rad} n_{exc}/I_{abs} = \gamma_{rad}/\gamma_{tot}$. In the following $Y_0 = \gamma^0_{rad}/\gamma^0_{tot}$ will denote the quantum yield of the SNP in the absence of MNPs, that is, before conjugation. In our simple model, we assume that the intrinsic SNP nonradiative rate $\gamma^0_{non-rad}$ is not affected by the metal-subsystem, whereas the parameters γ_{rad}, $\gamma_{non-rad,metal}$, and I_{abs} depend on the presence of metal. It is known that the light-emission and -absorption properties of SNPs can be modified strongly in the presence of metal

$$I_{abs} = P(\omega_{laser})\cdot I^0_{abs} \text{ and } \gamma_{rad} = P(\omega_{emiss})\cdot\gamma^0_{rad}$$

where $I^0_{abs}(\gamma^0_{abs})$ are the parameters in the absence of the metal NPs and $\omega_{emiss}(\omega_{laser})$ are the exciton-emission (excitation laser) frequencies. $P(\omega)$ is the electromagnetic-field enhancement factor

$$P(\omega) = \frac{\langle|\bar{E}_{actual}|^2\rangle_{\Omega,t}}{\langle E^2_{nometal}\rangle_t} \quad (1)$$

This factor includes the actual electric field $\vec{E}_{actual}$ inside the SNP, averaged over the volume of the SNP: $\bar{E}_{actual} = V^{-1}_{SNP} \int \vec{E}_{actual}\, dV$, where V_{SNP} is the volume of the SNP. Here $E_{nometal}$ is the laser electric field inside the SNP in the absence of MNPs. Another average $\langle ...\rangle_{\Omega,t}$ is taken over solid angle Ω and time; in the above formula, Ω is the solid angle defined for the direction of external laser field $\vec{E}_0$. To average over Ω in the numerical calculations, we use the following formula: $\langle|\bar{E}_{actual}|^2\rangle_{\Omega,t} = 1/3(\langle|\bar{E}_{actual,x}|^2\rangle_t + \langle|\bar{E}_{actual,y}|^2\rangle_t + \langle|\bar{E}_{actual,z}|^2\rangle_t)$, where the vector $\bar{E}_{actual,i}$ $(i = x,y,z)$ is the actual electric field inside the SNP created by the external laser field $\bar{E}_0|\vec{i}$ $(\vec{i} = \vec{x},\vec{y},\vec{z})$. Then the emission intensity is written as

$$I_{emiss}(\omega_{emiss}) = \frac{P(\omega_{emiss})\cdot\gamma^0_{rad}\cdot P(\omega_{laser})\cdot I^0_{abs}}{P(\omega_{emiss})\cdot\gamma^0_{rad} + \gamma^0_{non-rad} + \gamma_{non-rad,metal}(\omega_{emiss})} \quad (2)$$

The coefficients $P(\omega_{emiss(laser)})$ should be found numerically. $\gamma_{non-rad,metal}(\omega_{emiss})$ can be found starting from Fermi's golden rule:

$$\gamma_{non-rad,metal}(\omega_{exc}) = \frac{2\pi}{\hbar}\langle\sum_f |\langle 0_{exc}; f|\hat{V}_{int}|exc;0_{pl}\rangle|^2 \delta(\hbar\omega_{exc} - \hbar\omega_f)\rangle \quad (3)$$

In the above matrix elements, the initial state $|exc;0_{pl}\rangle$ describes an exciton in a SNP, and the final states $(|0_{exc}; f\rangle)$ contain the plasmon excitation in the MNP and no exciton in the SNP. The energies of the above states are denoted as $\hbar\omega_{exc}$ and $\hbar\omega_f$. The average $\langle ...\rangle$ is taken over all initial states of the exciton $|exc\rangle$ with energy $\hbar\omega_{exc}$. The operator for the Coulomb interaction between carriers in different NPs has the usual form: $\hat{V}_{int} = \sum_{i,j}\hat{V}_{Coul}(\vec{r}_i,\vec{r}_j)$, where $\vec{r}_i$ is the position of an electron inside the SNP participating in the exciton, and $\vec{r}_j$ are positions of the carriers inside the MNPs relative to the SNP. Here $\hat{V}_{Coul}(\vec{r}_i,\vec{r}_j)$ should be calculated as a potential energy of two electrons including the dielectric constant of the SNP, which is defined as: $\epsilon_1(\vec{r}) = \epsilon_{SNP}$ inside the SNP and $\epsilon_1(\vec{r}) = \epsilon_0$ ouside. In other words, the potential $\hat{V}_{Coul}(\vec{r}_i,\vec{r}_j)$ includes the effect of bound charges on the surface of SNP. Neglecting the coherent coupling between the exciton and plasmon, we factorize the wave functions $(|exc;0_{pl}\rangle = |exc> |0_{pl}\rangle$ and $|0_{exc}; f\rangle = |0_{exc}> |f\rangle)$

$$\sum_f |\langle 0_{exc}; f|\hat{V}_{int}|exc;0_{pl}\rangle|^2 \delta(\hbar\omega_{exc} - \hbar\omega_f) \approx \sum_f |\langle f|\hat{U}_{int}|0_{pl}\rangle|^2 \delta(\hbar\omega_{exc} - \hbar\omega_f)$$

where $\hat{U}_{int} = \langle 0_{exc}|\hat{V}_{int}|exc\rangle$ is the electric potential energy created by the exciton. The last sum includes only the wave

function of the electron plasma in a MNP and can be calculated with the fluctuation dissipation theorem (FDT)[15]

$$\sum_f |\langle f|\hat{U}_{\rm int}|0_{\rm pl}\rangle|^2 \delta(\hbar\omega_{\rm exc} - \hbar\omega_f) = \frac{1}{2\pi}\int_{-\infty}^{+\infty} e^{i\omega_{\rm exc}t}\langle 0_{\rm pl}|\hat{U}_{\rm int}(t)\hat{U}_{\rm int}(0)|0_{\rm pl}\rangle\, dt = -\frac{1}{\pi}{\rm Im}F_{\rm exc}(\omega_{\rm exc})$$

where $F_{\rm exc}(\omega_{\rm exc}) = \int dV\cdot n(r)\cdot u_{\rm int}(r) = \int dV\cdot\rho(r)\cdot\Phi_{\rm int}(r)$, where $n(r)$ and $\rho(r)$ are the local nonequilibrium electron and charge densities, respectively ($\rho = en$). The function $F_{\rm exc}$ also includes the effective electric potential created by an exciton, $\Phi_{\rm int}(r) = u_{\rm int}(r)/e = \langle 0_{\rm exc}|\hat{V}_{\rm Coul}|{\rm exc}\rangle/e$. This response function, $F_{\rm exc}$, should be found by calculating the local nonequilibrium charge density $\rho(r)e^{-i\omega t}$ in the presence of the "external" potential $\Phi_{\rm int}(r)e^{-i\omega t}$ and then taking the integral $\int dV\cdot\rho(r)\cdot\Phi_{\rm int}(r)$. Here we also assume that the spread of exciton energies (fine structure) in a single SNP is much smaller than the width of the plasmon peak of MNPs. This condition is realized in the typical experimental systems.

The potential $\Phi_{\rm int}(r) = \langle 0_{\rm exc}|\hat{V}_{\rm Coul}|{\rm exc}\rangle/e$ depends on the exciton wave function which, in general, may have a complex form due to mixing of heavy and light holes in the valence band. Using the envelope-function approximation and the method to calculate the interband Coulomb matrix elements described in ref 16, we arrive at the following equation

$$\nabla\epsilon_1(\vec{r})\nabla\Phi_{\rm int}(\vec{r}) = 4\pi\cdot ed_{\rm exc}\frac{\partial\vec{D}(\vec{r}_e)}{\partial\vec{r}_e}$$

where the function $\rho_{\rm exc} = -ed_{\rm exc}[\partial\vec{D}(\vec{r}_e)/\partial\vec{r}_e]$ is the spatial charge distribution induced by exciton inside the SNP and $ed_{\rm exc}\vec{D}(\vec{r}_e)$ is the spatial distribution of dipole moment; $d_{\rm exc}$ is the interband dipole moment ($d_{\rm exc}$ is a few Å typically) and $\vec{D}(\vec{r}_e)$ is expressed through envelope wave functions in the framework of the Luttinger model.[17,18] For the sake of simplicity, we employ here simplified wave functions without the mixing between heavy- and light-hole states.[19] In other words, we take in the following: $\vec{D}(\vec{r}_e) = \vec{\alpha}\cdot\Psi_h^*\cdot\Psi_e$ and $\Psi_e = \Psi_h = \sin(\pi r/R_{\rm SNP})/(\sqrt{2R_{\rm SNP}\pi}\cdot r)$, where $R_{\rm SNP}$ is the radius of SNP and $\vec{\alpha}$ can be the three unit vectors along the x, y, and z axes. Because $\rho_{\rm exc} = -ed_{\rm exc}[\partial\vec{D}(\vec{r}_e)/\partial\vec{r}_e]$ is proportional to the spherical harmonic with $l = 1$, the function $\Phi_{\rm int}(\vec{r})$ outside a spherical SNP has the form of the dipole potential

$$\Phi_{\rm int}(\vec{r}) = \frac{ed_{\rm exc}\vec{r}\cdot\vec{\alpha}}{\epsilon_{\rm eff}r^3} \qquad (4)$$

where $\epsilon_{\rm eff} = (2\cdot\epsilon_0 + \epsilon_{\rm SNP})/3$. The exciton in a SNP can be found in three states ($\vec{\alpha}||x,y,z$) with equal probabilities. Therefore, we average over three directions. For a MNP complex symmetric under three transformations $x \to -x$, $y \to -y$, and, $z \to -z$, we obtain

$$\gamma_{\rm non-rad,metal}(\omega_{\rm exc}) = -\frac{2\pi}{\hbar}\frac{1}{\pi}\frac{{\rm Im}(F_x + F_y + F_z)}{3} \qquad (5)$$

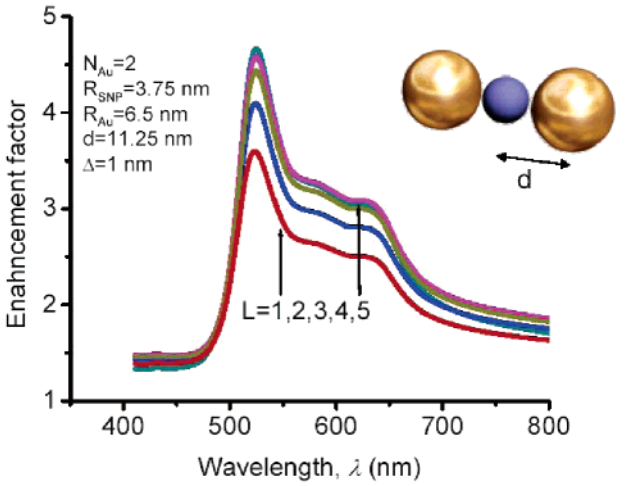

Figure 2. Calculated field enhancement factor of SNP conjugated with two Au NPs. The surface-to-surface distance, Δ, is just 1 nm.

where $F_\alpha = \int dV\cdot\rho_\alpha(r)\cdot\Phi_{{\rm int},\alpha}(r)$. The response function F_α is calculated for the exciton with α dipole moment ($\alpha = x,y,z$) and $\Phi_{{\rm int},\alpha}(\vec{r}) = ed_{\rm exc}r_\alpha/(\epsilon_{\rm eff}r^3)$.

In a system of several metal NPs, the response functions F_α must be calculated numerically. To do this, we will employ a multipole method and consider the near field regime $\lambda \gg d$, where λ is the wavelength of laser light. The resultant electric potential is found as $\varphi_{\rm tot} = \varphi_{\rm external}(t,\vec{r}) + \sum_n\varphi_n$, where $\varphi_{\rm external}(t,\vec{r}) = \varphi_{\rm ext}(\vec{r})e^{-i\omega t}$ and φ_n is the potential induced by the charges on the surface of the nth NP. The total potential should satisfy the near-field equation: $\nabla\epsilon(\vec{r})\nabla\varphi_{\rm tot} = 0$. The potentials of single NPs are expanded in terms of spherical harmonics

$$\varphi_n(\mathbf{r}) = \sum_{l,m} q_{l,m}^n \frac{Y_{l,m}(\theta_n,\phi_n)}{r_n^{l+1}} \qquad (6)$$

where $Y_{l,m}(\theta,\phi)$ are the spherical harmonics, $-l \le m \le l$, and the coordinates (θ_n,ϕ_n,r_n) are related to the coordinate system of the nth NP. Equation 6 is written for the potential outside of the nth NP. The standard boundary conditions are introduced at the surface of each NP and have the form: $\varphi_{\rm tot}|_{r=R_n+\delta} = \varphi_{\rm tot}|_{r=R_n-\delta}$ and $\epsilon_0(\partial\varphi_{\rm tot}/\partial r)|_{r=R_n+\delta} = \epsilon_n(\partial\varphi_{\rm tot}/\partial r)|_{r=R_n-\delta}$, where ϵ_n is the dielectric constant of the nth NP, ϵ_0 is the dielectric constant of the matrix, R_n is the radius of the nth NP, and $\delta \to 0$. The above boundary conditions are written for the nth NP and in the local coordinate system of the same NP. Application of the boundary conditions provides us with a infinite set of linear equations for the unknown coefficients $q_{l,m}^n$. To find the "multipole charges" $q_{l,m}^n$, we truncate the system of equations assuming that the $q_{l,m}^n$ decreases rapidly as a function of l. Therefore, we include only $l \le l_{\rm max}$. To calculate the electromagnetic-field enhancement factor $P(\omega)$ and response function $F(\omega)$, we will use the above numerical method. Below we will use $l_{\rm max} = 5$, which provides us with high precision of calculation even for tightly packed structures (the error is a few percent as shown in Figure 2).

For the case of $N_\gamma = 1$, we can obtain a convenient analytical equation in the dipole limit $d \gg R_{\rm SNP}, R_{\rm MNP}$, where

d is the distance between the metal and semiconductor NPs. In this case, we reduce the Coulomb potential to

$$\hat{V}_{\text{int}} = e^2/\epsilon_{\text{eff}} \sum_{i,j} \frac{(\vec{r}_{s,i}\cdot\vec{r}_j) - 3(\vec{r}_{s,i}\cdot\vec{n})(\vec{r}_j\cdot\vec{n})}{d^3}$$

where $\vec{d}$ is the vector connecting the NP centers, $\vec{n} = \vec{d}/d$, $\epsilon_{\text{eff}} = (2\cdot\epsilon_0 + \epsilon_{\text{SNP}})/3$. Then, the fluctuation−dissipation theorem generates the response function and we obtain a formula for the energy dissipation rate of an α exciton in a SNP due to a single MNP

$$\gamma_{\text{non-rad,metal},\alpha}(\omega_{\text{exc}}) = \frac{2}{\hbar} b_\alpha \frac{e^2\cdot d_{\text{exc}}^2}{d^6 \epsilon_{\text{eff}}^2} R_{\text{MNP}}^3 \cdot \text{Im}\left[\frac{\epsilon_\gamma(\omega_{\text{exc}}) - \epsilon_0}{\epsilon_\gamma(\omega_{\text{exc}}) + 2\epsilon_0}\right] \quad (7)$$

where the geometrical factor $b_\alpha = 1$, 1, and 4 for an α exciton with its dipole moment along $\vec{\alpha}||\vec{x},\vec{y}$, and $\vec{z}$, respectively; $\epsilon_\gamma(\omega)$ is the dielectric constant of metal (γ = Au or Ag) and Im $\epsilon_\gamma(\omega) > 0$; the inter-NP vector $\vec{d}$ is assumed in the z direction. By averaging over three exciton states, we obtain $\gamma_{\text{non-rad,metal}}(\omega_{\text{exc}})$ in the form of eq 7 with $b_{\text{aver}} = 2$.

To conclude this section, we briefly list the limitations of our approach. (a) The procedure (eq 6) to compute induced electric fields inside a NP complex is valid when the characteristic size of a NP complex is smaller that the wavelength of incident and emitted light. (b) Our model is based on the local dielectric constant and becomes less appropriate for very small NPs in which the surface creates additional damping for plasmons. (c) For very densely packed NP complexes, the method of spherical-harmonics expansion (eq 6) becomes less effective because we should sum over a large number of terms.

3. Gold−Semiconductor NP Molecule. Before calculating optical properties of many-NP assemblies, we are going to examine the energy transfer time from a semiconductor NP to a single Au nanocrystal ($N_{\text{Au}} = 1$). In the following, we will use the background dielectric constant of water ($\epsilon_0 = 1.8$) and the dielectric constant $\epsilon_{\text{Au}}(\omega)$ from empirical tables.[20] Figure 3 shows the calculated energy-relaxation times for the system studied in ref 9. The exciton dipole of CdSe NPs used in ref 9 can be estimated from the formula for the radiative lifetime:[21]

$$\gamma_{\text{rad}}^0 = \frac{8\pi\sqrt{\epsilon_0}\omega_{\text{exc}}^3 e^2 d_{\text{exc}}^2}{3(\epsilon_{\text{eff}}/\epsilon_0)^2 h\cdot c^3} \quad (8)$$

The measured parameters were as follows: $\gamma_{\text{tot}}^0 = 11$ns and $Y \approx 1$. From these numbers we obtain $d_{\text{exc}} = 2.7$Å. The data in Figure 3 were obtained by using the numerical calculations and eqs 4−6 (blue curve) and the dipole approximation of eq 7. We can see that the exact approach becomes progressively more important as the inter-NP distance decreases, in agreement with our expectations. At large distances $\gamma_{\text{non-rad,metal}} \propto 1/d^6$, whereas at small Δ and $R_{\text{MNP}} \gg R_{\text{SNP}}$ it becomes close to surface-transfer law $\gamma_{\text{non-rad,metal}} \propto 1/\Delta^4$.[22]

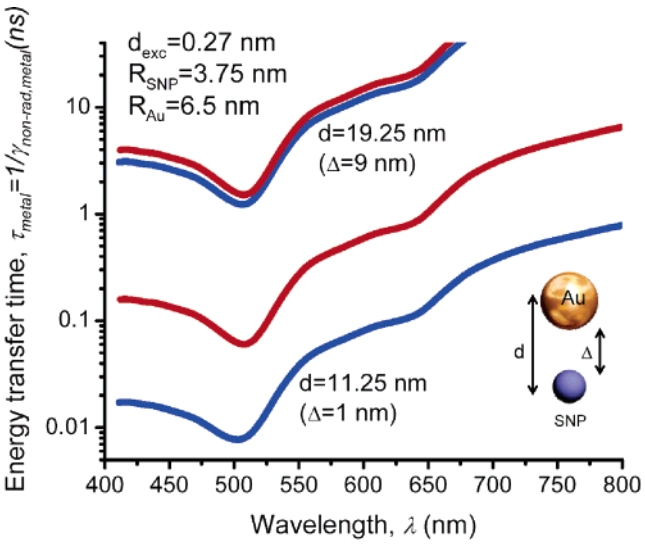

Figure 3. Energy transfer times in the hybrid molecule calculated with the numerical formalism (blue curves) and with dipole approximation (red curves). Inset: geometry of the system.

In Figure 4 we summarize the experimental transfer times taken from three publications[3,7,9] and compare them with our calculations. The parameters of the NPs are specified in the figure. The rate of energy dissipation is a strong function of the distance, d, exciton energy, and exciton dipole moment. The exciton dipole moment was estimated from eq 8. We see that for two cases[7,9] our approach using the bulk dielectric constant gives reasonable agreement between theory and experiment. The case of ref 3 stands alone: the discrepancy is more than 1 order of magnitude. This strong discrepancy was also pointed out by the authors of ref 3.

4. Gold−Semiconductor Assemblies. We now proceed to the more general case of $N_{\text{Au}} = N$ and $N_{\text{CdSe}} = 1$. Structures with $N_{\text{Au}} = 1-6$ were studied experimentally in ref 9. The parameters of the NP complex were: $R_{\text{Au}} = 6.5$ nm, $R_{\text{CdSe}} = 3.75$ nm, and $\Delta = 9$ nm, where Δ is the biolinker length.

To describe the emission process with eq 2, we computed the energy relaxation times and field enhancement factors for four symmetric complexes $N_{\text{Au}} = 1$, 2, 4, and 6 (Figure 5, upper part). The main conclusion is that, for the given parameters of the system studied in ref 9, the inter-NP Coulomb interaction is relatively weak and the enhancement factor at the important frequencies ($\omega_{\text{emiss(l)}}$) is about 1 (Figure 5b). In addition, the energy relaxation rates can be estimated well as $N_{\text{Au}}\cdot\gamma_{\text{non-rad,metal}}(\omega_{\text{exc}})$. To describe the change of emission due the MNPs, it is convenient to introduce the ratio of emission intensities before and after conjugation:

$$A(\omega_l,\omega_{\text{emiss}},N_{\text{Au}}) = \frac{I_{\text{emiss}}(N_{\text{Au}},\omega_{\text{emiss}})}{I_{\text{emiss}}(0,\omega_{\text{emiss}})} = \frac{P(\omega_l)\cdot P(\omega_{\text{emiss}})\cdot\gamma_{\text{tot}}^0}{P(\omega_{\text{emiss}})\cdot Y_0\cdot\gamma_{\text{tot}}^0 + \gamma_{\text{tot}}^0(1-Y_0) + \gamma_{\text{non-rad,metal}}(\omega_{\text{emiss}})} \quad (9)$$

For the NP assemblies realized in ref 9, the emission intensity of the SNP decreases gradually with the number of attached Au NPs (dots in Figure 5d). Our theory reproduces this behavior well.

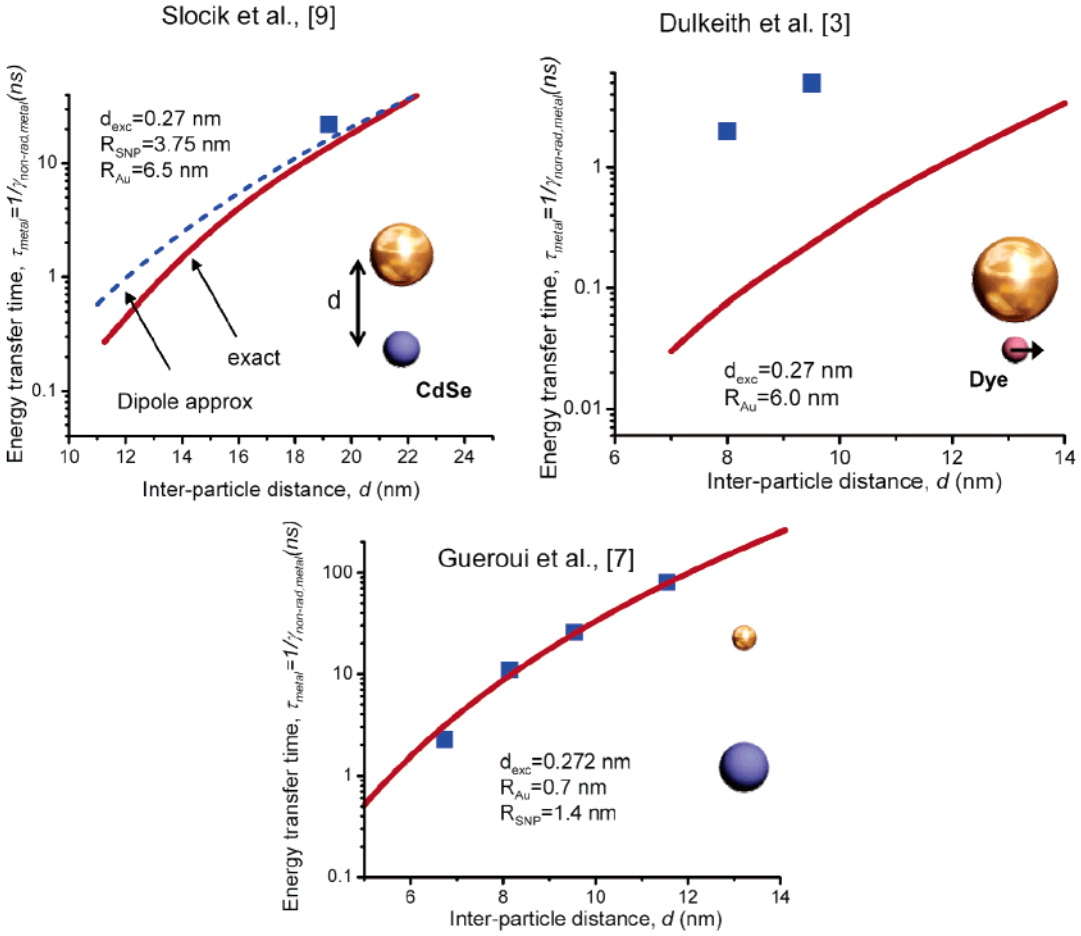

Figure 4. Energy transfer times as a function of the distance between CdSe and Au NPs in a hybrid molecule. The curves are calculated numerically, and symbols represent experimental data taken by three different groups. The blue curve in the upper left graph is calculated within the dipole approximation result (eq 7). Insets: geometry of the systems.

Furthermore, we study the emission intensity of the SNP as a function of its quantum yield. To do so in a consistent way, we keep the exciton recombination rate γ^0_{tot} constant and vary the quantum yield. Thus, the radiational rate becomes $\gamma^0_{rad} = \gamma^0_{tot} \cdot Y_0$ and $d_{exc} \propto \sqrt{Y_0}$. Note that, in this case, the energy transfer time becomes also dependent on Y_0: $\gamma_{non-rad,metal}(\omega_{emiss}) \propto d^2_{exc} \propto Y_0$. For CdSe NPs, the typical lifetime $1/\gamma^0_{tot}$ is about 11 ns. The CdTe NPs studied in a series of papers[4,13,14] have $\tau_{exc} \approx 20$ ns and relatively small quantum yield, $Y \approx 10\%$. For several cases presented here, we choose the parameters close to the experimental ones.

We will see from the results below that the quantum yield is an important parameter of the problem. If $Y_0 \approx 1$, eq 9 is reduced to

$$A(\omega_l,\omega_{emiss},N_{Au}) \approx P(\omega_l)\frac{P(\omega_{emiss})\cdot\gamma^0_{tot}}{P(\omega_{emiss})\cdot\gamma^0_{tot} + \gamma_{non-rad,metal}(\omega_{emiss})} \quad (Y_0 \approx 1) \quad (10)$$

It follows from the above formula that, if $Y_0 \approx 1$, then the emission enhancement (i.e., the case $A(\omega_l,\omega_{emiss},N_{Au}) > 1$) can be realized only in the regime of enhanced absorption when $P(\omega_l) > 1$. In the case $Y_0 \ll 1$ and $\gamma^0_{tot} \gg P(\omega_{emiss})\cdot\gamma^0_{rad} + \gamma_{non-rad,metal}(\omega_{emiss})$, we obtain

$$A(\omega_l,\omega_{emiss},N_{Au}) \approx P(\omega_l)\cdot P(\omega_{emiss}) \quad (Y_0 \ll 1) \quad (11)$$

In this case, an enhancement regime can also be achieved with an enhanced probability of photon emission when $P(\omega_{exc}) > 1$.

A more interesting situation occurs in the case of denser Au shells (Figure 6). We see some enhancement and it occurs if Y_0 is relatively small. This is according to eq 11 and reflects the fact that the intrinsic nonradiative rate $\gamma^0_{non-rad} = \gamma^0_{tot}(1 - Y_0)$ can be larger than $\gamma_{non-rad,metal}(\omega_{emiss}) \propto d^2_{exc} \propto Y_0$ even in the presence of several Au NPs. The possibility to enhance photoluminescence (PL) emission exists in Au-based complexes with an emitter of relatively small Y_0, about 1% (Figures 6d and 7). In addition, the wavelength of the emitter (SNP or dye) should be specially chosen. For the complex with $N_{Au} = 2$, a maximum PL intensity can be achieved for $\lambda_{emiss} \approx 650$ nm (Figure 7a). In the case of $N_{Au} = 4$, a maximum PL intensity is pushed toward longer wavelengths (Figure 7b). For the considered cases, the emission enhancement of Au-based assemblies comes from the increase of emission probability while the absorption of the incident photons does not change noticeably (Figure 6b).

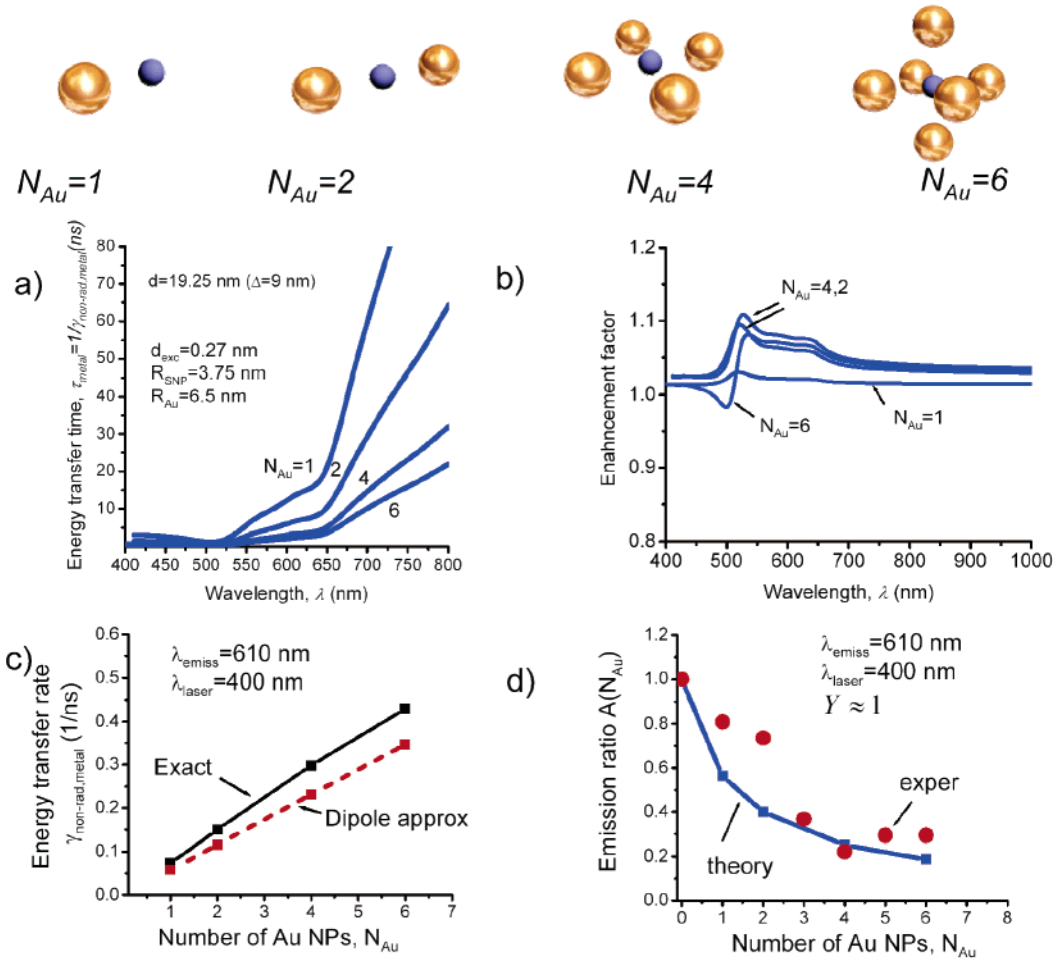

Figure 5. Energy transfer times (a) and enhancement factor (b) for the complexes assembled in ref 9. Parts c and d show energy transfer times and emission ratio as a function of number of MNP, respectively. The dots in part d represent the experimental data of ref 9. Upper part: geometry of the systems, shown to scale.

Hybrid complexes assembled with smaller building blocks can provide us with a wider variety of structures because the number of ways to arrange small NPs into a superstructure of a given size is larger. Figure 8 shows the data obtained for the structure with $N_{Au} = 54$ and $R_{Au} \approx 2$ nm. This structure incorporating a quantum emitter (CdSe NP) and Au shell has a complex spectrum of plasmon excitations strongly altered because of the inter-NP Coulomb interaction. The main plasmon peak in Figure 8a is blue shifted compared to the plasmon in a single Au NP (inset). The field enhancement factor in this structure is reduced in most wavelength intervals because of dynamic screening. The optical response is very sensitive to a size of MNP and inter-MNP spacing. In addition, energy relaxation is quite efficient. Therefore, PL intensity is suppressed in the presence of the Au crown. This structure can be used as a very efficient damper of SNP emission with sensor properties (see the next section).

5. Au-Based Assemblies with Sensor Properties. A type of sensor proposed in ref 14 utilizes a polymer as the inter-NP linker (Figure 9a and b). Some polymers, for example, poly(ethylene glycol) (PEG), are very sensitive to the environmental conditions such as, for example, temperature. Regarding the temperature response, PEG undergoes conformational phase transition in the temperature region $T = 30-60$ °C. In this temperature interval, its length increases rapidly with T and the total change in length is about 1 nm.[23] In a simplified approach, the T-dependence of the PEG length can be written as

$$\Delta = R_{PEG}(T) = 3 \text{ nm} + 1 \text{ nm } (T - 30 \text{ °C})/30 \text{ °C}.$$

Using the above equation, we obtain a simple formula for the radius of shell in Figure 9b: $R_{Shell}(T) = 11.8$ nm $+ R_{PEG}(T) = 14.8$ nm $+ (T - 30$ °C$)/30$ °C. CdTe NPs used in refs 13 and 14 have an exciton lifetime about 20 ns and $Y_0 \approx 10\%$. Using these parameters and eq 8, we obtain the following radiative dipole $d_{exc}(Y = 0.1) \approx 0.71$ Å ($\epsilon_{CdTe} = 7.2$).

A sensor mechanism observed in the Au−PEG−CdTe assemblies[14] can be explained in the following way: when the polymer (PEG) expands with temperature, the interaction between SNP and MNPs is changed. This change can be observed as an increase or decrease of the emission intensity, depending on the particular set of parameters. In the experiment,[14] the emission of SNP decreases as temperature increases. This observation was interpreted in ref 14 in terms of field enhancement at the exciton wavelength: the en-

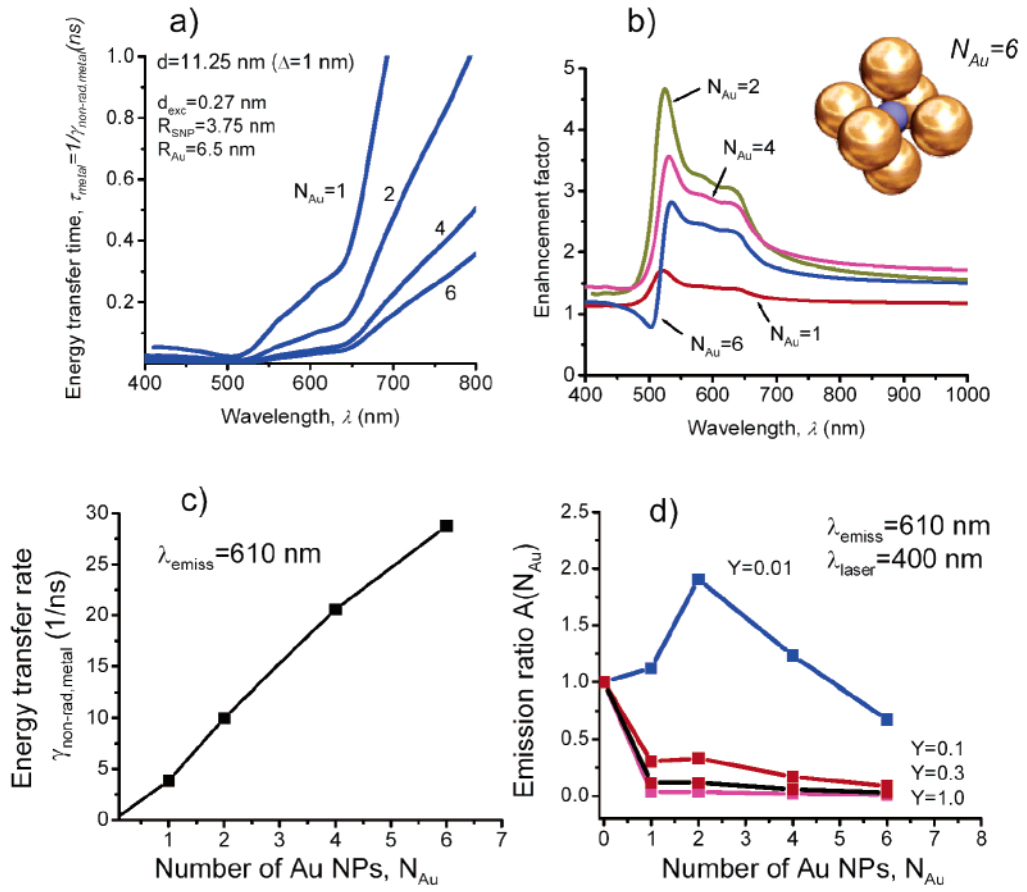

Figure 6. Energy transfer times (a) and enhancement factor (b) for Au-NP−CdSe-NP complexes with a denser NP packing. Energy transfer times (c) and emission ratio (d) for the complexes with $N_{Au} = 1-6$ and $N_{CdSe} = 1$. Inset: geometry of one of the complexes, shown to scale.

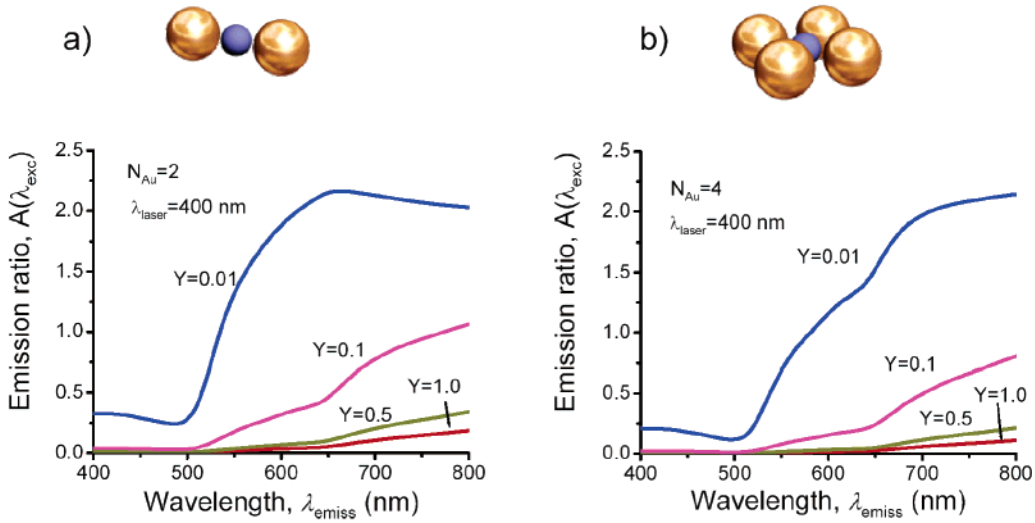

Figure 7. Emission ratios for Au-NP−CdSe-NP complexes with $N_{Au} = 2$ and 4 and $N_{CdSe} = 1$. Inset: geometry of one of the complexes, shown to scale.

hancement factor decreases rapidly with increasing radius R_{shell}, and therefore the emission intensity can also decrease with increasing Au−CdTe distance. Our theory in Figure 9c supports this possibility, giving an appreciable enhancement factor of about 2 at $\lambda_{emiss} \approx 600$ nm. However, we also must take into account the energy relaxation time, which grows with the linker length and therefore with temperature. The net temperature effect should incorporate both factors and depend on the specific set of parameters. For the typical parameters of the structures of ref 14, the calculated intensity decreases with temperature in agreement with experiment (Figures 9d and e). For calculations, we used a slightly increased background dielectric constant, $\epsilon_0 = 2.3$, to account for a polymer shell.

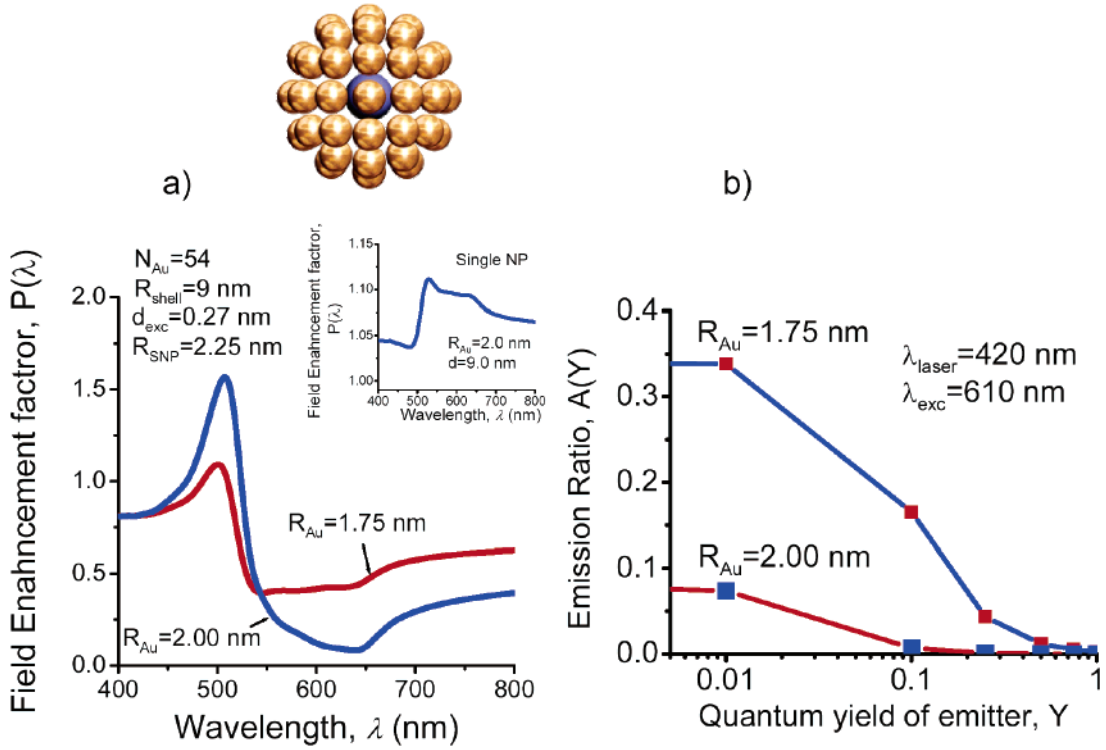

Figure 8. Optical characteristics of assemblies with 54 Au NPs and 1 CdSe NP. Inset: field enhancement factor due to a single Au NP. Upper part: geometry of the complex.

The enhancement factor in Figure 9c was calculated as an average over all polarizations of light (see eq 1). We should note that the field enhancement effect appears when the external electric field is along the axis joining the particles (x direction in Figure 9a). When the external electric field is perpendicular to this axis, the resultant field inside a SNP is reduced.[3]

The experiment[14] has several features: (A) In the experiment, the structure contains many SNPs (Figure 9b) and therefore excitons will flow from one NP to another via the Förster energy transfer mechanism. However, this transfer does not reduce the emission in a direct way because the number of excitons is conserved. (B) The excitation photon energy used in ref 14 is lower than the exciton peak ($\lambda_{laser} \approx$ 633 nm and $\lambda_{emiss} \approx$ 600 nm). Therefore, generation of excitons can partially arise through a two-photon absorption mechanism. Our formula (eq 2) is also applicable in this case because it describes the electric-field enhancement effect regardless of the specific absorption mechanism. (C) The CdTe−NP shell in the experiment[14] is disordered while our calculations are performed for an ideal shell. From the above discussion, we must conclude that the experimental system of ref 14 is complex and we should not overestimate our model. However, we think that our modeling gives important insight on the mechanisms of temperature-dependent emission and provides the principles to design nanocomplexes with tailored optical properties.

The inset in Figure 10 shows another structure with sensor properties. In this structure, the field enhancement factor is about one and the main mechanism of interaction between NPs is energy transfer. Therefore, emission intensity should increase with increasing linker length or with increasing temperature. This behavior is seen clearly in our calculations (Figure 10). In addition, we see in the inset of Figure 10 that the sensitivity of SNP emission to temperature grows with the number of MNPs.

We should also note that the T-sensitive emission mechanism in our structures comes from the conformational phase transition in the polymer linker. To reveal this mechanism in experiment, one has to be sure that the SNP emission itself is insensitive to the temperature. Such a background experiment was carried out in ref 14 and demonstrated that the CdTe SNPs used in the sensor structures do not change their emission in the important temperature range (ref 14, supplementary data).

For experiments in the linear optical regime, it is also important to be sure that the incident light does not heat the NP complex. Recent papers[24,25] provide us with a quantitative description of the heating process. For Au NPs with $R_{Au} <$ 20 nm and light intensity $I_{laser} < 10^4$ W/cm^2, the temperature increase at the surface of Au NP is less than a few degrees Celsius. At higher light intensities, the heating effect can become important.

6. Silver−Semiconductor Assemblies. Silver has a dielectric function, $\epsilon_{Ag}(\omega)$, very different from that of gold, and it is interesting to look at optical properties of Ag-based assemblies. Again, we use a dielectric constant of the bulk metal taken from ref 20. The results for a complex with $N_{Ag} = 54$ are shown in Figure 11. We again see that the plasmon frequency for the collective resonance is shifted to shorter wavelengths. Because Ag has a stronger plasmon resonance, Ag-based systems can provide larger enhancement factors than those provided by Au assemblies (compare Figures 8a and 11b). Because the plasmon peak is close to 400 nm, the

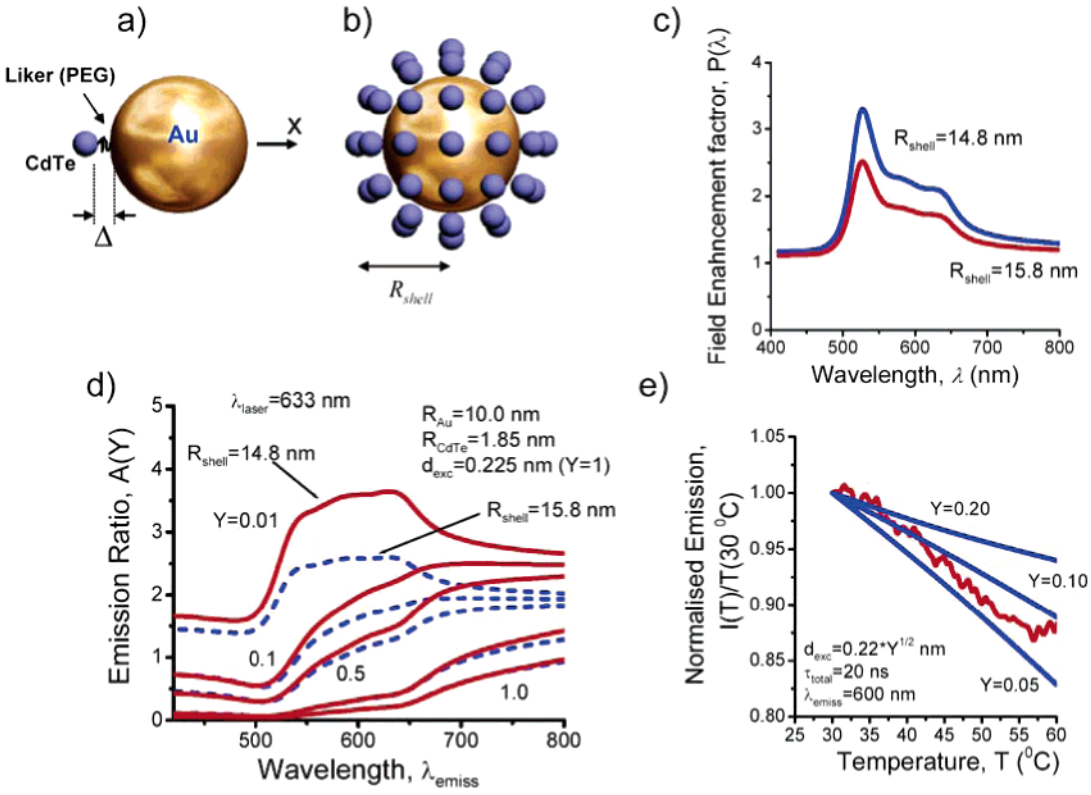

Figure 9. Schematics of a single SNP attached to a large Au NP (a) and NP complex assembled in ref 14 (b). Enhancement factor (c) and emission intensity (d) as a function of emission wavelength of a single CdTe NP in the complex (b) for two different polymer lengths. The excitation wavelength is $\lambda_{laser} \approx 633$ nm and $\lambda_{emiss} \approx 600$ nm, respectively. (e) Calculated normalized emission intensity as a function of temperature under the conditions of experiment 14 (blue). The red curve shows the experimental data from ref 14.

energy dissipation for the exciton at 600−700 nm is relatively weak. In these structures, strong enhancement can be achieved because of the increased absorption rate in the regime of the plasmon resonance ($\lambda_{laser} \approx 400$ nm), whereas the emission probability at $\lambda_{emiss} \approx 600-700$ nm is reduced slightly because of the dynamic screening in the structure[5] (Figure 11b and c). The resultant emission can be enhanced by a factor of 3 for $Y \approx 10\%$ (Figure 11c). Because the plasmon resonance in silver is so strong, assemblies based on Ag-NPs can demonstrate enhanced properties suitable for optical and sensor applications.

7. Discussion. It is interesting to compare the effects described here with SERS. It is known that Raman scattering signals in the presence of rough metal surface are enhanced dramatically (factors of $10^{10}-10^{14}$) permitting studies of single molecules (see, e.g., ref 26), and the photoluminescence intensity of SNPs is enhanced, at maximum, by a factor of 5−10.[4,10,11,14] This striking difference comes from two reasons. (1) The scales are different: SNPs are essentially larger than single molecules and to achieve field enhancement for SNPs one should enhance the field in all of the internal volume of a SNP. It is not so easy to realize this condition. The second reason is that PL includes incoherent processes such as fast intra-SNP energy relaxation and energy transfer to MNPs. It is also interesting to note that the emission enhancement was observed mostly in experiments with extended systems (rough metal surface, nanowires, large Au NPs) where the plasmon-induced field amplification can be especially strong. In most experiments with a few/several small Au NPs, the emission intensity decreases because of the energy transfer effect.

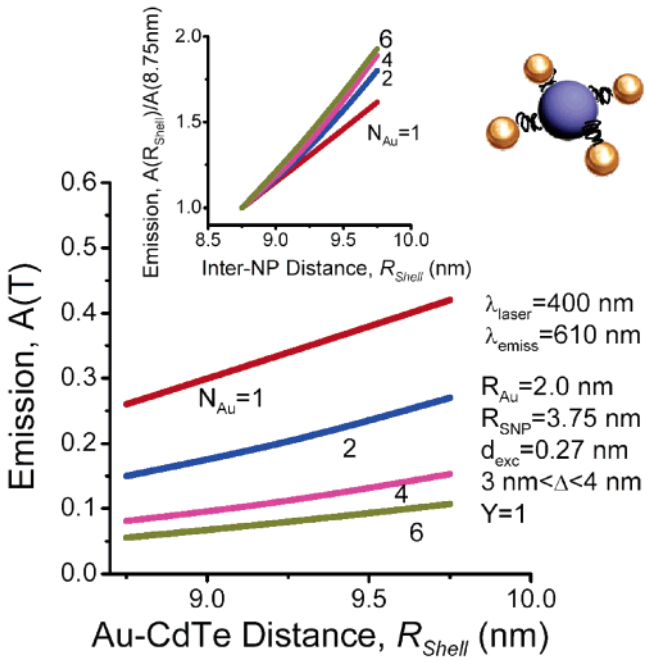

Figure 10. Calculated normalized emission intensity as a function of SNP−MNP distance; this change in biolinker size corresponds to the expansion of the polymer (PEG) as T increases from 30 to 60 °C. Left inset: normalized emission for different numbers of Au NPs attached to a CdSe NP. Right inset: schematics of the structure.

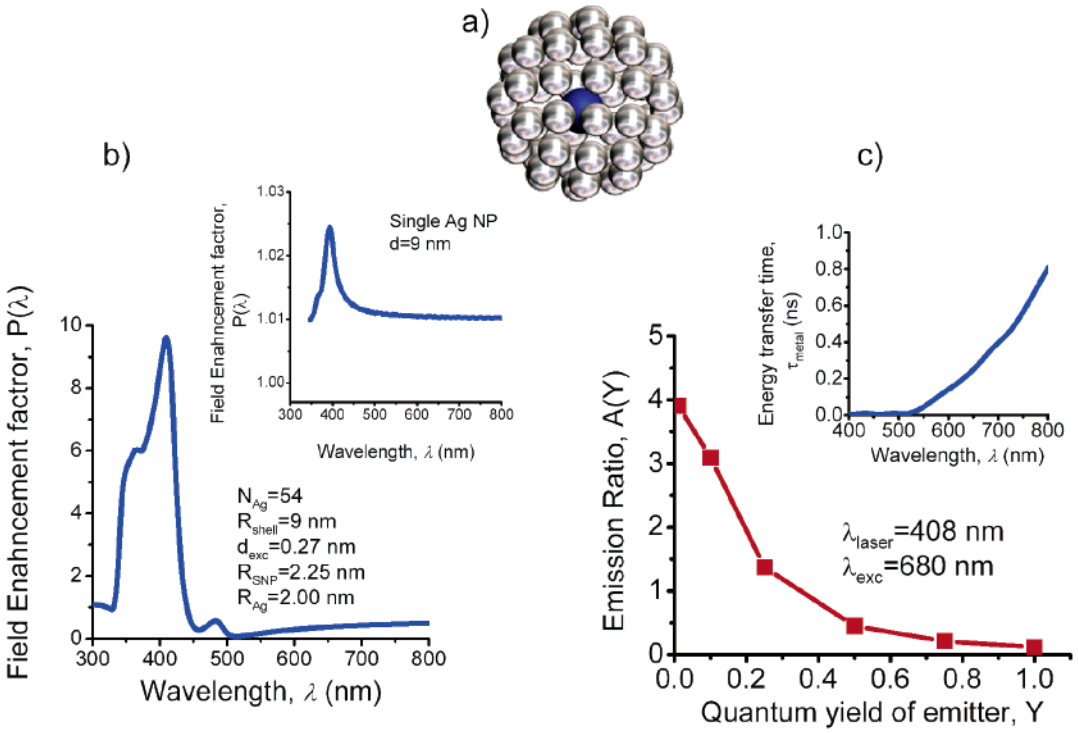

Figure 11. Optical characteristics of an assembly with 54 Ag NPs and 1 CdSe NP. (a) Schematics of the assembly. (b) Field enhancement factor of the complex with $N_{Ag} = 54$ and $N_{CdSe} = 1$. Inset: Field enhancement factor for the NP molecule $N_{Ag} = N_{CdSe} = 1$. (c) Emission of the complex $N_{Ag} = 54$ as a function of the emitter quantum yield. Inset: Energy transfer rate for the complex $N_{Ag} = 54$.

The energy transfer described in this paper is an incoherent process. Along with such incoherent processes, the interaction between metal and semiconductor NPs may have a coherent component. This coherent interaction can be understood as a process in which excitation is transferred back and forth between metal and semiconductor NPs. The exciton is converted into the plasmon and then back. The coherent interaction should occur in the vicinity of the exciton−plasmon resonance ($\hbar\omega_{exc} \approx \hbar\omega_{plasmon}$) and should lead to a shift of the exciton-emission frequency. To estimate this effect, we should use a quantum density-matrix formalism applied to a metal−semiconductor system.[27] The coherent shift of the exciton is proportional to a real part of the response function involved into eq 5: $\delta\omega_{exc} \approx (1/\hbar)\mathrm{Re}(F_x + F_y + F_z)/3$. The shift $\delta\omega_{exc}$ depends strongly on several parameters: $\epsilon_{metal}(\omega)$, N_{Au}, d_{exc}, d, and R_{MNP}. For the structures studied in this paper, we obtain $\delta\omega_{exc} = 0.01-100\ \mathrm{ns}^{-1}$. In optical studies of large collections of NPs at room temperature in a solution, a typical width of the exciton peak in PL spectra is about 100 meV, which is much greater than the estimated coherent energy shift $\hbar\delta\omega_{exc}$. Therefore, ensemble room-temperature measurements cannot reveal this type of interaction. We think that single-NP optical spectroscopy at low temperature could be a suitable method for observing the coherent component of exciton−plasmon interaction. We also should mention that the PL spectra of the Au-NP−CdTe-NP assemble[14] did not demonstrate a noticeable shift of the exciton peak, in agreement with the above estimations. At the same time, the experimental data on Au-conjugated CdTe nanowires showed clearly a blue shift for the exciton peak.[4] We think that this blue shift has a different physical origin and comes from spatial diffusion of photogenerated excitons along a nanowire.

To summarize, we have shown that optical emission of metal−semiconductor assemblies is modified strongly by interparticle Coulomb interaction. The important mechanisms of interaction are field enhancement and energy transfer. Because of the complexity of interparticle interactions in a complex made of few/many NPs, the emission intensity is a complex function of material and geometrical parameters and can be enhanced or suppressed during the process of conjugation. We also show that the emission of the system is sensitive to environmental parameters and that metal−semiconductor assemblies may have useful sensor properties.

Acknowledgment. This work was supported by NIST and BioNanoTechnology Initiative at Ohio University.

References

(1) Cui, Y.; Wei, Q.; Park, H.; Lieber, C. M. *Science* **2001**, *293*, 1289−1292.
(2) Yadong, Y. A.; Alivisatos, A. P. *Nature* **2005**, *437*, 664.
(3) Dulkeith, E.; Ringler, M.; Klar, T. A.; Feldmann, J.; Munoz Javier, A.; Parak, W. J. *Nano Lett.* **2005**, *5*, 585.
(4) Lee, J.; Govorov; A. O.; Dulka, J.; Kotov, N. A. *Nano Lett.* **2004**, *4*, 2323.
(5) Lee, J.; Govorov, A. O.; Kotov, N. A. *Agnew. Chem.*, submitted for publication.
(6) Kagan, C. R.; Murray, C. B.; Bawendi, M. G. *Phys. Rev. B* **1996**, *54*, 8633.
(7) Gueroui, Z.; Libchaber, A. *Phys. Rev. Lett.* **2004**, *93*, 166108.
(8) Yun, C. S.; Javier, A.; Jennings, T.; Fisher, M., Hira, S.; Peterson, S.; Hopkins, B.; Reich, N. O.; Strouse, G. F. *J. Am. Chem. Soc.* **2005**, *127*, 3115.
(9) Slocik, J. M.; Govorov, A. O.; Naik, R. R. *Supramol. Chem.*, in press.
(10) Shimizu, K. T.; Woo, W. K.; Fisher, B. R.; Eisler, H. J.; Bawendi, M. G. *Phys. Rev. Lett.* **2002**, *89*, 117401.

(11) Kulakovich, O.; Strekal, N.; Yaroshevich, A.; Maskevich, S.; Gaponenko, S.; Nabiev, I.; Woggon, U.; Artemyev, M. *Nano Lett.* **2002**, *2*, 1449.
(12) Jiang, J.; Bosnick, K.; Maillard, M.; Brus, L. *J. Phys. Chem. B* **2003**, *107*, 9964.
(13) Lee, J.; Govorov, A. O.; Kotov, N. A. *Nano Lett.* **2005**, *5*, 2064.
(14) Lee, J.; Govorov, A. O.; Kotov, N. A. *Angew. Chem.* **2005**, *117*, 7605.
(15) Platzman, P. M.; Wolf, P. A. *Waves and Interactions in Solid State Plasma*; Academic Press: New York, 1973.
(16) (a) Govorov, A. O. *Phys. Rev. B* **2005**, *71*, 155323. (b) Govorov, A. O. *Phys. Rev. B* **2003**, *68*, 075315.
(17) Bir, G. L.; Pikus, G. E. *Symmetry and Strain-Induced Effects in Semiconductors*; Wiley: New York, 1975.
(18) Baldereschi, A.; Lipari, N. O. *Phys. Rev. B* **1973**, *8*, 2697.
(19) A more sophisticated model based on the Luttinger Hamiltonian[17,18] would give a more complex form of the potential including higher spatial harmonics because of the mixing between heavy and light holes. Numerically, effect of mixing on the transfer matrix elements is relatively small.[16] In addition, for structures with dimension $d \gg R_{SNP}$ multipole contributions have additional small parameter R_{SNP}/d; here d is the distance between SNP and MNPs and R_{SNP} is the SNP radius. For several structures calculated here $d \gg R_{SNP}$ and higher harmonics can be neglected.
(20) Palik, E. D. *Handbook of Optical Constants of Solids*; Academic Press: New York, 1985.
(21) Yariv, A. *Quantum Electronics*, 2nd ed.; John Wiley & Sons: New York, 1975.
(22) Persson, B.; Lang, N. *Phys. Rev. B* **1982**, *26*, 5409.
(23) (a) Ferry, J. D. *Viscoelastic Properties of Polymers*, 3rd ed.; Wiley: New York, 1980. (b) Barton, A. F. M. *CRC Handbook of Polymer-Liquid Interaction Parameters*; CRC Press: Boca Raton, FL, 1990. (c) Munro, J. C.; Frank, C. W. *Langmuir* **2004**, *20*, 3339−3349.
(24) Govorov, A. O.; Zhang, W.; Skeini, T.; Richardson, H.; Lee, J.; Kotov, N. A. *Nanoscale Res. Lett.* **2005**, *1*, 100101.
(25) Richardson, H. H.; Hickman, Z. N.; Govorov, A. O.; Thomas, A. C.; Zhang, W.; Kordesch, M. E. *Nano Lett.* **2006**; DOI: 10.1021/nl060105l.
(26) Nie, S.; Emory, S. R. *Science* **1997**, *275*, 1102.
(27) Zhang, W.; Govorov, A. O.; Bryant, G. W., to be submitted for publication.

NL0602140